Model resolution of gross Rayleigh wave data

Jianghai Xia, Kansas Geological Survey, The University of Kansas; Chao Chen, China University of Geosciences*

Summary

The model resolution matrix (Wiggins, 1972) indicates that a model can be perfectly resolved in a least-squares sense if error-free data are inverted. High-frequency (≥ 2 Hz) Rayleigh wave data are utilized to determine shear (S)-wave velocities in near-surface geophysics. Gross Rayleigh wave data in this abstract are specifically referred to high-frequency Rayleigh wave phase velocities that are contaminated by errors. The errors can be introduced during data acquisition and/or by artifacts of data processing. The errors in data are equivalent to a smear matrix in the model space that reduces the model resolution. The degree of smear in a model is dependent on data accuracy. Because of the smear matrix, an S-wave velocity model obtained by inversion of Rayleigh wave phase velocities in the real world cannot be perfectly resolved. However, the resolution power of gross Rayleigh wave data can be ascertained after the data accuracy is determined.

Introduction

Shear (S)-wave velocities can be derived from inverting dispersive phase velocities of the surface (Rayleigh and/or Love) wave (e.g., Aki and Richards, 1980, p. 664). Stokoe and Nazarian (1983) presented a surface-wave method, Spectral Analysis of Surface Waves (SASW), which analyzes the dispersion curve of the ground roll to produce near-surface S-wave velocity profiles. Another research project (Park et al., 1999; Xia et al., 1999) utilizes a multichannel recording system to estimate near-surface S-wave velocity from high-frequency (≥ 2 Hz) Rayleigh waves (Multichannel Analysis of Surface Waves—MASW). This research has been expanded to analyze the effects of higher modes on inversion of surface waves and investigation depth (Xia et al., 2003; Beaty et al., 2002) and the feasibility of estimating near-surface quality factors (Q) by inverting attenuation coefficients of Rayleigh waves (Xia et al., 2002a). The differences between MASW results and direct borehole measurements are 15% or less and random (Xia et al., 2002b). The selection of field data acquisition parameters for MASW was theoretically studied by Zhang et al. (in press). MASW applications in near-surface geophysics can be found in numerous publications (e.g., Xia et al., 1998, 2002b and 2002c; Ivanov et al., 2000; Miller et al., 1999; Yilmaz and Eser, 2002, and Tian et al., in press).

The fundamental question of model resolution with high-frequency Rayleigh wave data still remains. Understanding the model resolution in inversion of Rayleigh wave phase velocities is critical in applying the MASW method to near-surface geological/geophysical problems. The model resolution matrix (Wiggins, 1972) provides a numerical criterion that evaluates how well the true model parameters can be resolved. We will show that gross data introduces a smear matrix in the model space so it indeed reduces the model resolution. Given data accuracy, therefore, a potential resolution of gross Rayleigh wave data can be calculated by forward modeling based on physical properties and the spatial location of a target and surrounding materials.

Model resolution

Near-surface S-wave velocities can be estimated by inverting phase velocities of high-frequency Rayleigh waves (Xia et al., 1999 and 2003). Near-surface quality factors (Q) can also be determined by inverting attenuation coefficients of Rayleigh waves (Xia et al., 2002a). Both algorithms are based on the overdetermined system

$$\mathbf{G}\mathbf{m}^{true} = \mathbf{d}, \tag{1}$$

where $\mathbf{G}$ is an $m \times n$ matrix ($m > n$ in both cases), and $\mathbf{m}^{true}$ and $\mathbf{d}$ are model and data vectors, respectively. $\mathbf{G}$ stands for a data kernel that embodies $\mathbf{m}^{true}$ and experimental geometry. Letting $\mathbf{H}$ be a generalized inverse of $\mathbf{G}$, we get an estimated model $\mathbf{m}^{est}$

$$\mathbf{m}^{est} = \mathbf{H}\mathbf{d}. \tag{2}$$

Substituting Equation (1) into Equation (2), we obtain

$$\mathbf{m}^{est} = \mathbf{H}\mathbf{d} = \mathbf{H}[\mathbf{G}\,\mathbf{m}^{true}] = [\mathbf{H}\mathbf{G}]\mathbf{m}^{true} = \mathbf{R}\mathbf{m}^{true}. \tag{3}$$

Matrix $\mathbf{R}$ is the $m \times m$ model resolution matrix (Wiggins, 1972). The resolution matrix is only determined by the data kernel and the a priori information added to the problem. It is therefore independent of actual values of the data (Menke, 1984). Equation (3) shows the estimated model parameters $\mathbf{m}^{est}$ are weighting averages of the true model parameters $\mathbf{m}^{true}$ (Figure 1). The weighting function is the matrix $\mathbf{R}$. For example, the ith estimated model parameter $m_i^{est} = \sum_{j=1}^{n} r_{ij} m_j^{true}$, where r_{ij} is the jth element of the ith row of matrix $\mathbf{R}$. If $\mathbf{R} = \mathbf{I}$ ($\mathbf{I}$ is the unit matrix), each model parameter is uniquely determined so it reaches the highest resolution possible.

The least-squares solution used in Xia et al.'s work (1999, 2002a, and 2003) would possess the highest model resolution because the generalized inverse of the solution in the least-squares sense is $\mathbf{H} = [\mathbf{G}^T\mathbf{G}]^{-1}\mathbf{G}^T$. The resolution matrix $\mathbf{R}$ is

$$\mathbf{R} = \mathbf{HG} = [\mathbf{G}^T\mathbf{G}]^{-1}\mathbf{G}^T\mathbf{G} = \mathbf{I}. \quad (4)$$

Equation (4) shows model parameters can be perfectly resolved. This is the result we normally obtained when applying an inverse algorithm that is based on a least-squares sense to "pure" data (data without any noise).

In the real world, measured data are inevitably contaminated by noise from different sources and/or noise introduced by processing procedures. The gross data are "pure" data $\mathbf{d}$ with noise $\Delta\mathbf{d}$. Equation (1) becomes

$$\mathbf{G}\mathbf{m}^{est} + \mathbf{G}\Delta\mathbf{m} = \mathbf{d} + \Delta\mathbf{d}, \quad (5)$$

where $\Delta\mathbf{m}$ is the error in the estimated model $\mathbf{m}^{est}$ and is introduced by errors $\Delta\mathbf{d}$. $\Delta\mathbf{m}$ can be expressed in $\mathbf{m}^{est}$

$$\Delta\mathbf{m} = \mathbf{E}\mathbf{m}^{est}, \quad (6)$$

where $\mathbf{E}$ is an m $\times$ m non-zero matrix. We call it a "smear" matrix. The smear matrix always exists because there are m variables (a row vector of $\mathbf{E}$) in each equation so that $\mathbf{E}$ can almost freely be selected to be any matrix and not necessarily a diagonal matrix. Using Equation (6) to rewrite Equation (5), we can easily understand how contaminated data reduce the model resolution.

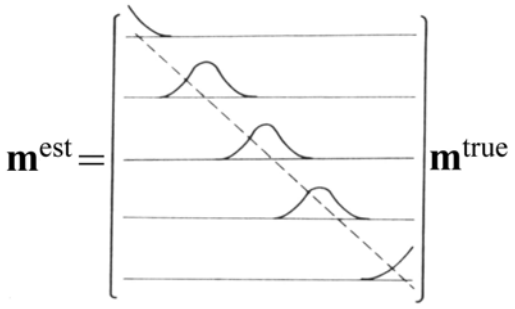

Figure 1. The model resolution matrix R. The narrow peaks along the main diagonal of the matrix indicate that the model is well resolved. The best scenario is that R is the unit matrix that means the model is completely determined (from Menke, 1984).

$$\mathbf{G}\mathbf{m}^{est} + \mathbf{G}\Delta\mathbf{m} = \mathbf{G}\mathbf{m}^{est} + \mathbf{G}\mathbf{E}\mathbf{m}^{est} = \mathbf{G}(\mathbf{I} + \mathbf{E})\mathbf{m}^{est}. \quad (7)$$

The resolution matrix of the linear system (7) in a least-squares sense will be

$$\mathbf{R} = \mathbf{HG} = [\mathbf{G}^T\mathbf{G}(\mathbf{I} + \mathbf{E})]^{-1}\mathbf{G}^T\mathbf{G} = (\mathbf{I} + \mathbf{E})^{-1}[\mathbf{G}^T\mathbf{G}]^{-1}\mathbf{G}^T\mathbf{G} = (\mathbf{I} + \mathbf{E})^{-1} \neq \mathbf{I}. \quad (8)$$

The resolution matrix is no longer the unit matrix so that the estimated model $\mathbf{m}^{est}$ (= $\mathbf{R}\mathbf{m}^{true}$) truly becomes the weighting average of the true model. The errors in data $\Delta\mathbf{d}$ are transmitted into the inverted model by the smear matrix $\mathbf{E}$ so that the model resolution is reduced. Although it is not possible in most cases to determine the smear matrix $\mathbf{E}$, it is clear that the resolution of an inverted model is reduced because of arbitrariness of $\mathbf{E}$ that is introduced by errors in data $\Delta\mathbf{d}$.

Modeling results

Discussion in the previous section shows the smear matrix $\mathbf{E}$ introduced by errors in data reduces the model resolution. In other words, the model resolution is limited by the data accuracy. If the maximum response of an anomalous layer (e.g., a low/high velocity layer in the half-space) is weaker than the data errors, it is impossible to detect this layer because the smear matrix $\mathbf{E}$ reduces the model resolution to the level at which the layer cannot be distinguished from the half-space. For a given data accuracy, therefore, the resolving power of geophysical data can be determined by the forward modeling.

We used a two-layer model (left, Figure 2) with one layer on top of the half-space as a background model (a solid line) to demonstrate the resolution power of Rayleigh wave phase velocities. Model 1 (solid dots) consists of a low velocity layer (50% lower than the background model) from depths of 1.5 m to 3.5 m that replaces the background model at these depths. The maximum relative change in Rayleigh wave phase velocities is 34% at 45 Hz (right, Figure 2). If the maximum relative data error is less than 34%, an inversion of Rayleigh wave data (e.g., Xia et al., 1999; Beaty et al., 2002) could resolve the low velocity layer. Otherwise, the inversion of Rayleigh wave data cannot detect this low velocity layer. We moved the low velocity layer a little deeper to 7.5 m to 9.5 m (solid triangles, Model 2). The maximum relative change in Rayleigh wave phase velocities is 32% (right, Figure 2). Again, if the maximum relative data error is less than 32%, an inversion of Rayleigh data could resolve the low velocity layer in this setting. It is worth pointing out that the maximum relative change is shifted from 45 Hz to 17 Hz as the center depth of the low velocity layer is moved from 2.5 m to 8.5 m. To focus our attention on the maximum relative change in Rayleigh wave phase velocities we only plot the maximum relative change of Rayleigh wave phase velocities, as the low velocity layer is in different settings in the following modeling results and we ignore the frequency at which the maximum relative change occurs. These results provide more comprehensive insight into the relationship between the resolution and the data accuracy.

Contour maps (Figure 3) show the maximum relative changes in Rayleigh wave phase velocities as a low velocity layer changes its central depth and its thickness. We modeled a low velocity layer in the background model (Figure 2) in two settings, an S-wave velocity of a low velocity layer is a 25% or 50% lower than the background model. For the former case, the maximum relative changes of Rayleigh wave phase velocities vary from less than 5% to more than 40% depending on depth to the layer and the thickness of the layer. For example, to resolve a 2-m thick layer at depth of 6 m (indicated by a star in the left of Figure 3), the maximum relative change of Rayleigh wave phase velocities is approximately 14%. If the error level (the maximum relative error) of Rayleigh wave phase velocities (measured data) is less than 14%, inverse algorithms should theoretically be able to

detect this low velocity layer because measured data still possess enough resolving power. On the other hand, if the error level of measured data is higher than 14%, inverse algorithms are not able to detect this low velocity layer because measured data no longer possess enough resolving power. It is well known, however, that a higher velocity contrast makes detecting an anomalous layer easier. The accuracy requirement for measured data will be dramatically reduced in detecting a low velocity layer if its S-wave velocity contrast increases. For example, in the later case (right, Figure 3), for a low velocity layer with the same thickness at the same depth as the former case but its velocity contrast being 50% (a star in the right of Figure 3), inverse algorithms can resolve the layer only requiring an error level of less than 30%. An error level, however, must be reduced below 15% to resolve a 1-m thick layer (a solid dot in the right of Figure 3). A trend of changes in Rayleigh wave phase velocities with S-wave velocity contrasts can be demonstrated by Figure 4.

Contour maps (Figure 4) show the maximum relative changes in Rayleigh wave phase velocities as a low velocity layer within the background model (Figure 2) changes its depth and a velocity contrast. To resolve a 1-m thick layer with a 30% S-wave velocity contrast at depth of 6 m (a star in the left of Figure 4), an error level of measured data must be less than 9%. The accuracy requirement for measured data will be reduced in detecting a low velocity layer if the thickness of the layer increases. For example, if its thickness increases to 2 m, an error level of measured data could be as high as 18% (a star in the right of Figure 4). As indicated by a solid dot in the right of Figure 4, when a velocity contrast increases to 50%, the error tolerance to detect this low velocity layer could reach around 32%.

Conclusions

The smear matrix introduced by errors in measured data limits the resolving power of geophysical data. The way to increase the model resolution is to increase the accuracy of measured data. Modeling results are based on the layered earth model so they can provide the vertical resolution of surface wave techniques in near-surface applications. It is necessary to perform the forward modeling of high-frequency Rayleigh waves during the designing phase of a data acquisition plan to define upper limits of an error level. Measured data whose errors are below the error level secure an inverted model possessing a certain resolution that is sufficient for geological interpretation. Feeding poor data into inverse algorithms can only produce unrealistic models.

Acknowledgements

We appreciate Mary Brohammer for her assistance in manuscript preparation.

References

Aki, K., and Richards, P.G., 1980, Quantitative seismology: W.H. Freeman and Company, San Francisco.

Beaty, K.S., Schmitt, D.R., and Sacchi, M., 2002, Simulated annealing inversion of multimode Rayleigh wave dispersion curves for geological structure*: Geophys. J. Int*., 151**,** 622–631.

Ivanov, J., Park, C.B., Miller, R.D., Xia, J., Hunter, J., Good, R.L., and Burns, R.A., 2000, Joint analysis of surface-wave and refraction events from river-bottom sediments: Technical Program with Biographies, SEG, 70th Annual Meeting, Calgary, Canada, 1307-1310.

Menke, W., 1984, Geophysical data analysis--Discrete inversion theory: Academic Press, Inc., New York.

Miller, R.D., Xia, J., Park, C.B., and Ivanov, J., 1999, Multichannel analysis of surface waves to map bedrock: *The Leading Edge*, 18, 1392-1396.

Park, C.B., Miller, R.D., and Xia, J., 1999, Multichannel analysis of surface waves: *Geophysics*, 64, 800-808.

Tian, G., Steeples, D.W., Xia, J., Miller, R.D., Spikes, K.T., and Ralston, M.D., in press, Multichannel analysis of surface wave method with the Autojuggie: *Soil Dynamics and Earthquake Engineering.*

Stokoe II, K.H., and Nazarian, S., 1983, Effectiveness of ground improvement from Spectral Analysis of Surface Waves: Proceeding of the Eighth European Conference on Soil Mechanics and Foundation Engineering, Helsinki, Finland.

Wiggins, R.A., 1972, The general linear inverse problem: Implication of surface waves and free oscillations for Earth structure: *Rev. Geophys. Space Phys*., 10, 251-285.

Xia, J., Miller, R.D., and Park, C.B., 1998, Construction of vertical section of near-surface shear-wave velocity from ground roll: Technical Program, The Society of Exploration Geophysicists and The Chinese Petroleum Society Beijing 98' International Conference, 29-33.

Xia, J., Miller, R.D., and Park, C.B., 1999, Estimation of near-surface shear-wave velocity by inversion of Rayleigh wave: *Geophysics*, 64, 691-700.

Xia, J., Miller, R.D., Park, C.B., and Tian, G., 2002a, Determining *Q* of near-surface materials from Rayleigh waves: *Journal of Applied Geophysics*, v. 51, no. 2-4, 121-129.

Xia, J., Miller, R.D., Park, C.B., Hunter, J.A., Harris, J.B., and Ivanov, J., 2002b, Comparing shear-wave velocity profiles from multichannel analysis of surface wave with borehole measurements: *Soil Dynamics and Earthquake Engineering*, v. 22, no. 3, 181-190.

Xia, J., Miller, R.D., Park, C.B., Wightman, E., and Nigbor, R., 2002c, A pitfall in shallow shear-wave refraction surveying: *Journal of Applied Geophysics*, v. 51, no. 1, 1-9.

Xia, J., Miller, R.D., Park, C.B., and Tian, G., 2003, Inversion of high frequency surface waves with fundamental and higher modes: *Journal of Applied Geophysics*, v. 52, no. 1, 45-57.

Yilmaz, O., and Eser, M., 2002, A unified workflow for engineering seismology: Technical Program with Biographies, SEG, 72nd Annual Meeting, Salt Lake City, UT, 1496-1499.

Zhang, S.X., Chan, L.S., and Xia, J., in press, The selection of field acquisition parameters for dispersion images from multichannel surface wave data: *Pure and Applied Geophysics.*

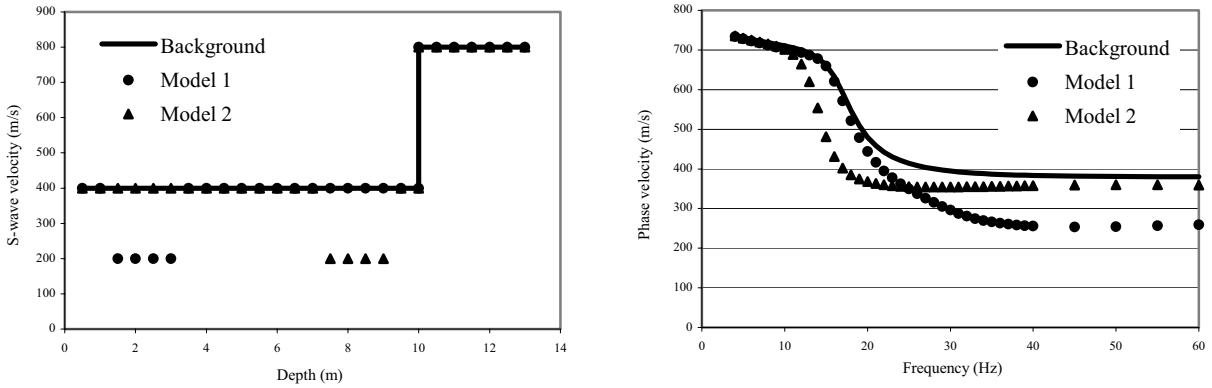

Figure 2. A low velocity layer at a different depth (solid dots and triangles, left) within a two-layer model (a solid line, left) and their Rayleigh wave phase velocities (right). The P-wave velocity and the density of the two-layer model are 800 m/s and 1,750 kg/m^3 for the top layer, and 1,600 m/s and 2,000 kg/m^3 for the half-space, respectively.

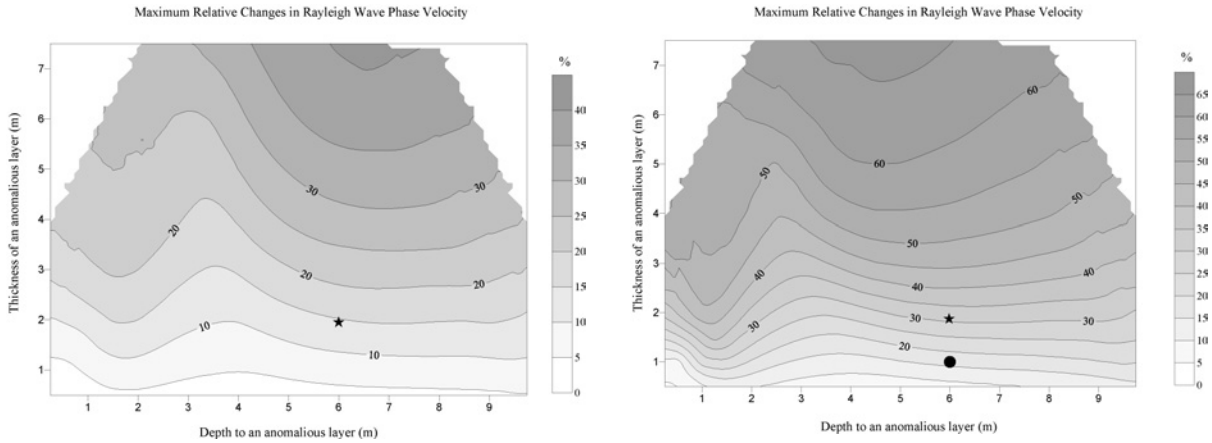

Figure 3. Contour maps show the maximum relative changes in Rayleigh wave phase velocities as a low velocity layer, with (left) an S-wave velocity that is a 25% lower than the background model (a solid line in the left of Figure 2) and with (right) an S-wave velocity that is a 50% lower than the background model, changes its central depth (x-axis) and its thickness (y-axis). See text for the explanation of stars and the dot.

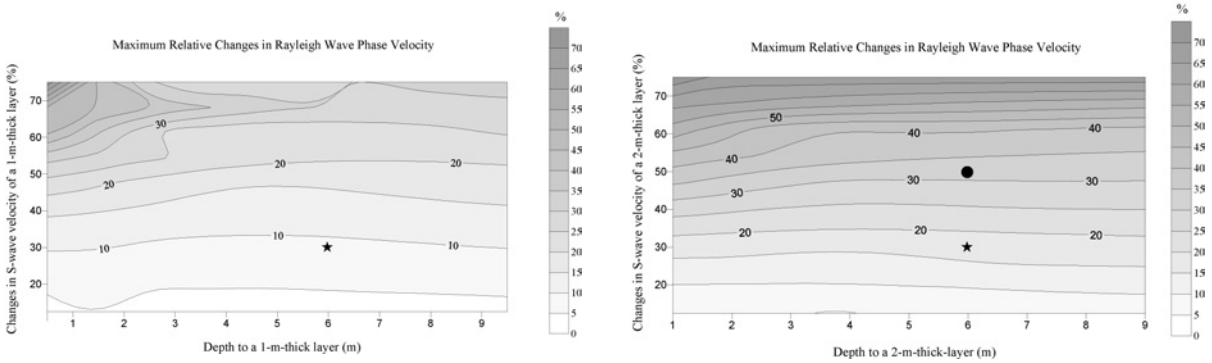

Figure 4. Contour maps show the maximum relative changes in Rayleigh wave phase velocities as a low velocity layer, (left) with one-meter thickness and (right) with two-meter thickness, changes its central depth (x-axis) and the percentage that is lower than background velocity (y-axis). See text for the explanation of stars and the dot.